RSC Advances

PAPER

View Article Online
View Journal | View Issue

Cite this: *RSC Adv.*, 2026, **16**, 29940

A composite lateral flow test substrate by capillary deposition of cellulose on synthetic paper

Qinghao He,†[a] Jiahua Zhong,†[a] Haonan Li,[a] Xionghui Li,[a] Yixi Shi,[a] Muyang Zhang,[a] Jie Zhou,[a] Hao Chen,[a] Xinyi Chen,[a] Zhuoting Han,[b] Lok Ting Chu,[c] Huiru Zhang*[d] and Weijin Guo *[a]

Lateral flow test (LFT) has been a very popular platform for point-of-care testing (POCT). Traditionally, LFT uses (nitro)cellulose or microstructured polymer as the substrate. In this work, we develop a new LFT substrate by capillary deposition of cellulose on a microstructured polymer substrate off-stoichiometry thiol–ene (OSTE) synthetic paper, which is formed by interlocked slanted OSTE micropillars. This substrate has uniform thickness and stable lateral flow rate with customized design. The lateral flow rate can be adjusted by changing the dimensions of the LFT test strip, the concentration of deposited cellulose, or the Tween 20 concentration in cellulose to meet specific requirements. Spotting tests are conducted on this substrate to facilitate the following immobilization of immuno reagents. We successfully use this substrate in various applications including urine glucose detection (an enzyme-based immunoassay), iodate detection of saline solutions, and plasma separation from whole blood, which proves this substrate has enormous potential for LFT in POCT.

Received 14th February 2026
Accepted 25th May 2026

DOI: 10.1039/d6ra01317a

rsc.li/rsc-advances

1 Introduction

Point-of-care testing (POCT) refers to tests that can be performed at bedside any time when needed, which do not require specialized equipment and personnel.[1] Compared to traditional laboratory tests, POCT greatly simplifies the testing process while maintaining its essential steps. Consequently, patients and physicians can obtain test results with greater ease and expediency, thus reducing the time and financial expenditures on testing.[2] Currently, POCT has been extensively implemented and achieved a high degree of acceptance among patients due to its convenience and high precision.[3]

As a representative of POCT, lateral flow tests (LFT) have been a very popular and successful platform with enormous applications in various fields, including pregnancy test, infectious disease detection,[4,5] environmental monitoring,[6,7] drug abuse[8] and food safety testing.[9–11] The common substrate material of LFT is cellulose or nitrocellulose.[12–14] Both of cellulose and nitrocellulose employ their own fiber structure to facilitate passive fluid transportation by autonomous capillary pumping.[15,16] Because of the low cost, easy manufacturing and portability of (nitro)cellulose, LFT by (nitro)cellulose stand out as an affordable platform for POCT.[17–20] Conventional processes for fabricating LFT generally involve patterning barriers and establishing flow channels on (nitro)cellulose substrate.[21,22] The methods of patterning paper based LFT substrates include screen printing,[23,24] flexographic printing,[25] inkjet printing,[26] wax printing,[27] laser printing,[28] chemical vapor deposition,[29,30] wet etching,[31] and capillary deposition.[32]

Although (nitro)cellulose paper is suitable and popular as the substrate material of LFT, further applications of them are limited by their non-uniform microstructures, strong autofluorescence, and unstable capillary flow. Recently researchers have tried to use microstructure polymer as the substrate of LFT, targeting to improve the performance of LFT substrate in microstructure, autofluorescence and capillary flow rate. Jönsson *et al.* developed a polymer pillar forest substrate by injection molding of cycloolefin-copolymer, enabling stable contact angles and demonstrating utility in a high-performance C-reactive protein LFT.[33] Melin *et al.* demonstrated a successful application of this LFT substrate in multiplexed detection of C-reactive protein and N-terminal pro-brain natriuretic peptide.[34] Han *et al.* developed a hybrid substrate made of paper and soluble polymers, offering advantages of low cost, scalability, and high sensitivity, while enabling automated data reading.[35] Liu *et al.* proposed a surface-structured membrane that successfully enables rapid self-transport of water through convection. This approach reduces residual samples on the membrane surface and achieves high sensitivity in lateral flow

[a]*Department of Biomedical Engineering, Shantou University, Shantou, 515063, Guangdong, China. E-mail: guoweijin@stu.edu.cn*

[b]*Department of Laboratory Medicine, The Second Affiliated Hospital of Guangdong Medical University, Zhanjiang, 524003, China*

[c]*Institute of Biochemistry and Molecular Biology, Guangdong Medical University, Zhanjiang, 524023, Guangdong, China*

[d]*Neusoft Institute Guangdong, Foshan, 528225, Guangdong, China. E-mail: zhanghuirugd@foxmail.com*

† These authors contributed equally to this work.

immunoassays.[36] Xu *et al.* added dimethyl sulfoxide (DMSO) to the LFA strip, which caused changes in the substrate structure. This treatment successfully induced gelation and high transparency of the porous NC membrane.[37] Off-stoichiometry thiol–ene (OSTE) synthetic paper, consisting of interlocked OSTE micropillars, were developed as a novel LFT substrate with uniform microstructures and clinically relevant capillary flow rates.[38] OSTE synthetic paper has also shown its superior performance in surface chemistry enabling covalent bonding of immuno reagents, and autofluorescence weaker than nitrocellulose.[39] Guo *et al.* reported the application of OSTE synthetic paper for efficient plasma separation from whole blood,[40] and colorimetric detection of glucose in a LFT fashion.[41] Although these microstructured polymer substrates have shown their potential as the substrate of LFT, their specific surface area is less than (nitro)cellulose, which could be an obstacle limiting their wider applications.

In this work, for the first time, we develop a composite LFT substrate which combines the porous cellulose and microstructured polymer together by depositing cellulose on OSTE synthetic paper. OSTE synthetic paper serves as the base, and the internal void of synthetic paper is filled by cellulose. This composite substrate is expected to obtain the uniform microstructure of OSTE synthetic paper and the high specific surface area of cellulose at the same time. For the fabrication of this composite substrate, firstly OSTE synthetic paper is fabricated by multi-directional photolithography of polymer OSTE.[42] Secondly, we deposit the cellulose solution onto synthetic paper, and cellulose solution will fill the porous synthetic paper by capillary action. Finally, we remove excess cellulose by wiping to ensure uniform thickness of porous cellulose in synthetic paper. We show that the substrate has a fine microstructure, uniform thickness, and stable capillary flow rate, which can be easily controlled by adjusting the dimensions of the micropillars of synthetic paper, the concentration of deposited cellulose, or the Tween 20 concentration in cellulose. In addition, this substrate is low-cost, easy to manufacture, and can be easily fabricated with a customized shape, all of which make this substrate ideally suited for LFT. As a proof of concept, we prepare a LFT based on this composite substrate for colorimetric detection of glucose in urine to verify the lateral flow performance and practicality of our substrates in POCT. Furthermore, we design a device to evaluate iodate concentration in food salt to demonstrate the wide scalability of this substrate. Lastly, we build a LFT device by this substrate to efficiently separate plasma from whole blood, to demonstrate the potential of our substrate in handling of complex biological samples. Overall, we believe that this work will provide a new strategy for preparing a LFT substrate that balances cost and performance.

2 Experiments

2.1 Materials

Polymer OSTE-Thiol (40) is prepared according to the previous work.[42] Hydrophobic spray is from Veslee (Guangzhou, China). Microcrystalline cellulose (50 μm) is from Aladdin (Shanghai, China). Tween 20, isopropanol, phosphoric acid, sodium chloride, potassium iodate, potassium iodide and soluble starch are bought from Macklin (Shanghai, China). Hydrochloric acid and acetone are bought from Ghtech (Guangzhou, China). Dialysis film is from Ronmark Technology (Shenzhen, China). Nitrocellulose membrane is from Cobetter (NC140C, Hangzhou, China). Color dye is from Guangxi Juliheng Biotechnology (Nanning, China). Glucose is from Xilong Scientific (Shantou, China). Peroxidase from horseradish and glucose oxidase from aspergillus are bought from Sigma (USA). DAB substrate kit is from Biosharp (Hefei, China). Blood group typing reagent (agglutinating antibody) is from Solarbio (Beijing, China).

2.2 Fabrication of the composite substrate

Fabrication procedures of the composite substrate are shown in Fig. 1. Firstly, we prepare a piece of plastic film. Then a thin film of OSTE with a thickness of 200 μm is fabricated on the plastic film. After that, we fabricate the OSTE interlocked slanted micropillars using the multi-directional photolithography of OSTE by a chromium mask (see Fig. S1), followed by development by isopropanol and acetone. After post flood UV cure, we get a piece of synthetic paper (12.0 cm × 12.0 cm). For the dimensions of micropillars of synthetic paper, we test three dimensions in total: SP1: the diameter of micropillars is 100 μm, the center-to-center distance of micropillars is 200 μm, and the thickness of micropillars is 200 μm, SP2: the diameter of micropillars is 150 μm, the center-to-center distance of micropillars is 300 μm, and the thickness of micropillars is 200 μm, SP3: the diameter of micropillars is 200 μm, the center to-center distance of micropillars is 400 μm, and the thickness of micropillars is 200 μm.

For the capillary flow experiments, we stick test strips by the composite substrate on a 3D printed setup. Water solution with green color dye is added from the front end of the test strips. The whole capillary flow is captured and analyzed by software Tracker (https://opensourcephysics.github.io/tracker-website/).

The cellulose suspension used in this work was prepared following a protocol modified from Ma *et al.*[32] For the detailed procedures (see Fig. S2), firstly we mix 10.0 mL 37% hydrochloric acid and 1.0 g microcrystalline cellulose by dropping hydrochloric acid on microcrystalline cellulose. Then we stir the mixture at room temperature for 2 hours. After that, we put it into a dialysis bag and soak the bag in DI water until the pH value becomes 7.0. Lastly, the cellulose solution is removed from the dialysis bag and stored in a glass bottle.

For the patterning of cellulose on synthetic paper, at first we prepare synthetic paper test strips of 6.0 mm × 40 mm. Then, synthetic paper is treated by plasma cleaner to make it hydrophilic. Tween 20 is added in cellulose solution before deposition. Capillary action enables the autonomous filling of cellulose solution into the porous space of synthetic paper. The patterning volume density of cellulose solution on synthetic paper is 1.67 μL mm^{-2}. After the cellulose solution is fully dry on synthetic paper, the composite substrate is ready for experiments. The ambient temperature and humidity of the experiments are about 20–25 °C and 30–40%. The photolithographic

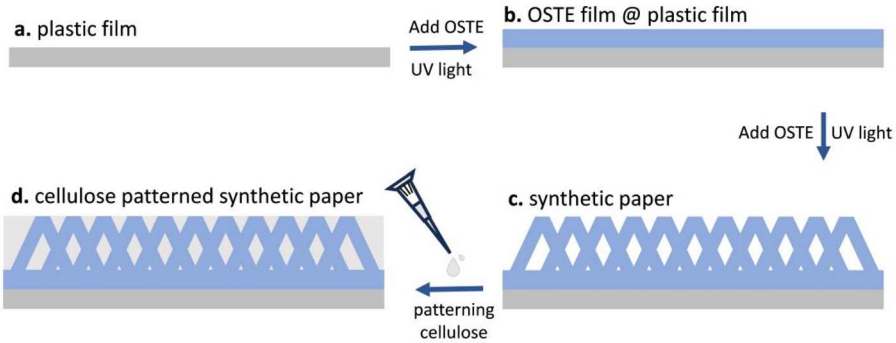

Fig. 1 The fabrication of the composite substrate by capillarily depositing cellulose on OSTE synthetic paper. (a) A piece of plastic film is prepared as the base. (b) A thin layer of OSTE film is prepared on the plastic film. (c) OSTE interlocked slanted micropillars are prepared on the OSTE film by the multi-directional photolithography of OSTE. (d) Cellulose is patterned on OSTE synthetic paper by depositing cellulose solution on synthetic paper and drying.

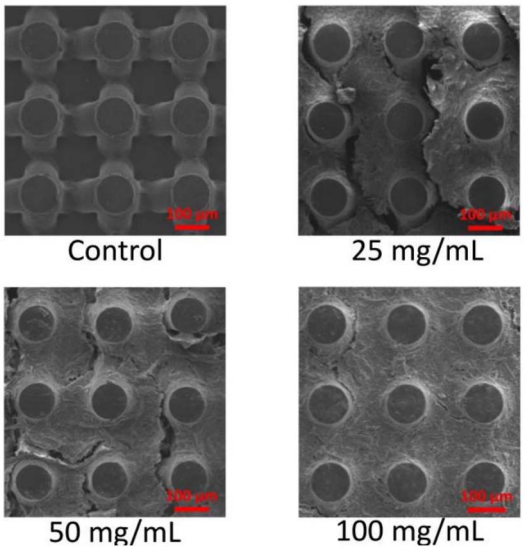

Fig. 2 SEM images of test strips by SP1 with different cellulose concentrations. The cellulose concentrations are 0 (control), 25 mg mL^{-1}, 50 mg mL^{-1} and 100 mg mL^{-1} respectively. The concentration of Tween 20 is 0.02%.

OSTE micropillars are accurate and stable. The height of the cellulose is equal to the height of the OSTE micropillars, so there is little difference between different batches of test strips.

2.3 Sample preparation

In the capillary flow experiment, we use the composite substrate by three synthetic papers (SP1, SP2, and SP3) for investigation. Firstly, we investigate the influence of synthetic paper dimensions on the capillary flow rate. Secondly, we investigate the influence of cellulose concentration on the capillary flow rate. With the same condition of Tween 20 concentration (0.02% volume of cellulose solution), we pattern cellulose solutions of different concentration on synthetic paper respectively. To be specific, the concentration of cellulose includes 100 mg mL^{-1}, 50 mg mL^{-1} and 25 mg mL^{-1}. Lastly, we investigate the influence of Tween 20 on the capillary flow rate. With the same concentration of cellulose (100 mg mL^{-1} cellulose) on synthetic paper, we adjust the concentration of Tween 20, including 0.02%, 0.05% and 0.1%.

2.4 Spotting test on the composite substrate

To facilitate the patterning of immuno reagents on the composite substrate, we investigate the relationship between the patterning area and the reagent volume. Firstly, different concentrations (100 mg mL^{-1}, 50 mg mL^{-1} and 25 mg mL^{-1}) of cellulose suspension are added on synthetic paper to fabricate different test strips. Then, 0.25 μL, 0.5 μL and 1.0 μL of solutions with green color dye are added on each type of test strips. After that, these test strips are left to fully dry and scanned by a color scanner (Epson, Japan). ImageJ (https://imagej.net/ij/) is used to analyze the size of these spots.

2.5 Glucose detection in urine

Fresh urine samples are collected from healthy volunteers, and glucose is spiked in the samples in order to prepare urine samples with glucose concentrations of 0 mM, 2.0 mM, 4.0 mM, 8.0 mM, 12.0 mM and 16.0 mM respectively. Synthetic paper is cut into a rectangle shape as 25.0 mm × 4.0 mm. A detection area with a size of 4.0 mm × 4.0 mm at one end is used as the colorimetric detection area. Cellulose solution is exclusively added in the detection area. DAB (10.0 μL Reagent A and 10.0 μL Reagent B of DAB kit are added into 200 μL DI water to get DAB solution) and enzymes (GOx concentration: 900 units per mL, HRP concentration: 1200 units per mL) are mixed together as glucose detection reagent. The volume ratio of DAB, glucose oxidase (GOx) and horseradish peroxidase (HRP) is 10 : 1 : 1. 4.8 μL glucose detection reagent is added on the cellulose detection area. After the test strips are fully dry, urine samples with different glucose concentrations are added on the other end of the test strips without cellulose. Waiting for 5 minutes, the color of the detection area changes to brown. We scan the test strip and analyze the intensity of blue channel of the detection area by ImageJ.

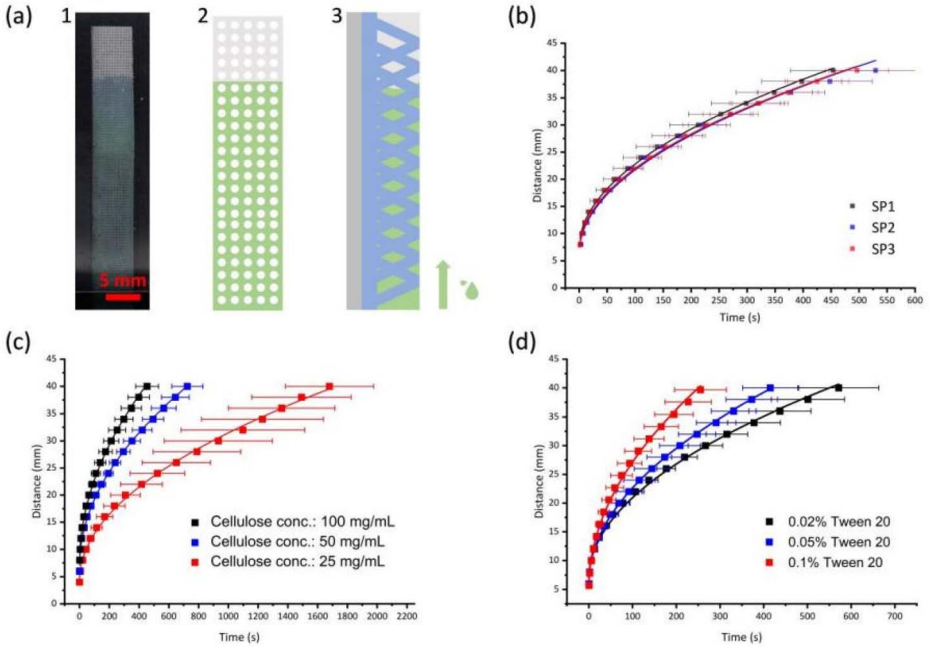

Fig. 3 Capillary flow behaviors of water on different types of test strips by the composite substrate. Each experiment is repeated at least 6 times. (a) The diagrams of capillary flow on the test strip. (1) is a picture of water flow on the test strip. (2) and (3) are the schematic top view and side view of capillary flow on the test strip. (b) shows the capillary flow behaviors on test strips by SP1, SP2 and SP3 with cellulose concentration as 100 mg mL^{-1} and Tween 20 concentration as 0.02%. The fitting by Washburn equation on SP1 test strips: distance $= 1.556 \times t^{0.5} + 7.242$, with R^2 as 0.9982. The fitting by Washburn equation on SP2 test strips: distance $= 1.544 \times t^{0.5} + 6.288$, with R^2 as 0.9927. The fitting by Washburn equation on SP3 test strips: distance $= 1.527 \times t^{0.5} + 6.741$, with R^2 as 0.9974. (c) shows the capillary flow behaviors on the test strips by SP1 with cellulose concentration of 100 mg mL^{-1}, 50 mg mL^{-1} and 25 mg mL^{-1}. In addition, the concentration of Tween 20 is 0.02%. The fitting by Washburn equation on the test strips of 100 mg mL^{-1} cellulose: distance $= 1.556 \times t^{0.5} + 7.242$, with R^2 as 0.9982. The fitting by Washburn equation on test strips of 50 mg mL^{-1} cellulose: distance $= 1.233 \times t^{0.5} + 6.847$, with R^2 is 0.9988. The fitting by Washburn equation on test strips of 25 mg mL^{-1} cellulose: distance $= 0.8605 \times t^{0.5} + 4.268$, with R^2 as 0.9983. (d) shows the capillary flow behaviors on test strips by SP1 with 0.02%, 0.05% and 0.1% Tween 20. In addition, the concentration of cellulose is 100 mg mL^{-1}. The fitting by Washburn equation on the test strip with 0.02% Tween 20: distance $= 1.416 \times t^{0.5} + 6.781$, with R^2 as 0.9963. The fitting by Washburn equation on the test strip with 0.05% Tween 20: distance $= 1.658 \times t^{0.5} + 6.075$, with R^2 as 0.9991. The fitting by Washburn equation on the test strip with 0.1% Tween 20: distance $= 2.074 \times t^{0.5} + 7.450$, with R^2 as 0.9975.

2.6 Iodate detection in salt

We prepare test strips (10.0 mm × 10.0 mm) by the composite substrate for the detection of iodate ion in food salt. Firstly, an equal volume of 6% starch solution is mixed with 0.08 M potassium iodide (KI) solution, which serves as the colorimetric reagent. Potassium iodate standard solutions with concentrations of 20.0 mg L^{-1}, 40.0 mg L^{-1}, 60.0 mg L^{-1}, 80.0 mg L^{-1} and 100.0 mg L^{-1} are prepared respectively. Potassium iodate standard solutions, NaCl solution (0.15 M) and phosphoric acid solution (0.5 M) are mixed with the ratio 1 : 3:1 to form NaCl solution containing iodate. 20.0 μL of colorimetric reagent is dropped onto the test strips and fully dried in the fume hood. Then, 200 μL of NaCl solution is added on the test strips. Later, we take the images of the test strips after fully reaction and use ImageJ for data analyze.

2.7 Plasma separation from whole blood

We prepare a synthetic paper test strip by a cutting plotter (Graphtec, Japan) with a circular sampling area, a narrow flow channel for plasma collection and a collecting region. The radius of sampling area is 12.5 mm. The size of flow channel is 15.0 mm × 2.0 mm. The collecting area is 5.0 mm × 2.0 mm. 4.0 μL cellulose solution is exclusively patterned on the collecting area. Firstly, 35.5 μL blood agglutination antibody is added on the sampling area for 4 times to ensure enough amount of the antibody. Then the test strip is left to fully dry. 40.0 μL human blood samples of corresponding type with HCT of 40% are added to the sampling area. The experimental video is recorded for data analysis. Human whole blood samples are collected from health volunteers, approved by the ethics committee of the Second Affiliated Hospital of Guangdong Medical University, complying with Declaration of Helsinki and Ethical Review Measures for Biomedical Research Involving Human Subjects of China. Informed consents are obtained from all participants.

3 Results and discussions

3.1 Microstructures of the composite substrate

After the deposition and fully dry of cellulose on synthetic paper, the composite substrate by synthetic paper and cellulose is formed. Fig. 2 shows the microstructures of the composite

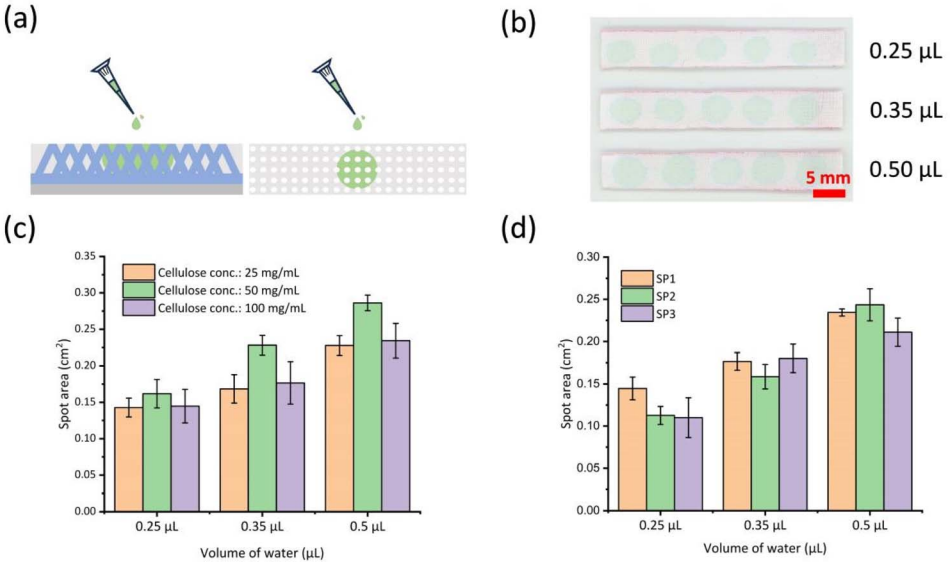

Fig. 4 Spot size after dropping 0.25 μL, 0.35 μL and 0.5 μL water on different test strips. Each experiment is repeated at least 6 times. (a) The diagrams of spot size after dropping water on test strip. (b) Pictures of spots on the test strips. The test strip is fabricated by patterning 100 mg mL^{-1} cellulose on SP1. Water of 0.25 μL, 0.35 μL and 0.5 μL is added to the test strips respectively. (c) shows the spot sizes on test strips with cellulose concentration of 25 mg mL^{-1}, 50 mg mL^{-1}, and 100 mg mL^{-1}. When 0.25 μL water is added on the test strips, the average areas are 0.1427 cm^2, 0.1618 cm^2, and 0.1447 cm^2. When 0.35 μL water is added on the test strips, the average areas are 0.1684 cm^2, 0.2282 cm^2, and 0.1766 cm^2. When 0.50 μL water is added on the test strips, the average areas are 0.2278 cm^2, 0.2862 cm^2, and 0.2344 cm^2. (d) shows the spot sizes on test strips by SP1, SP2, and SP3. When 0.25 μL water is added on the test strips, the average areas are 0.1447 cm^2, 0.1126 cm^2, and 0.1100 cm^2. When 0.35 μL water is added on the test strips, the average areas are 0.1766 cm^2, 0.1586 cm^2, and 0.1802 cm^2. When 0.50 μL water is added on the test strips, the average areas are 0.2344 cm^2, 0.2435 cm^2, and 0.2110 cm^2.

substrates by depositing cellulose of different concentrations on SP1. Compared to control group (synthetic paper alone), the composite substrates have cellulose filling the gap between OSTE pillars. With the increase of cellulose concentration, the cellulose becomes smoother and more compact, with fewer cracks. Through SEM images, the crack length of cellulose with different concentrations is labeled and calculated. It can be seen from images that when the cellulose concentration is 25 mg mL^{-1}, 50 mg mL^{-1} and 100 mg mL^{-1}, the average crack lengths are 1077.87 μm, 896.89 μm and 303.48 μm respectively, as shown in Fig. S3.

3.2 Capillary flow on the composite substrate

Fig. 3 shows the capillary flow behaviors of water on test strips by the composite substrate with different dimensions of synthetic paper, different concentrations of cellulose solution,

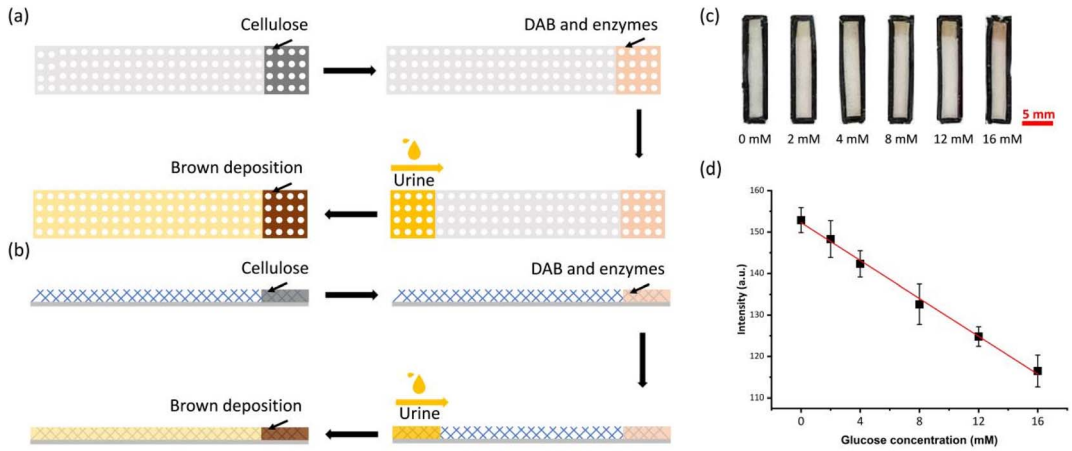

Fig. 5 Glucose detection in urine. (a) Experimental procedures of glucose reaction (top view). DAB and enzymes are added on the test strip, and then urine samples are added to flow to the reaction zone. (b) is the side view of the experimental procedures. (c) Brown precipitations of different intensity are produced with different glucose concentrations. (d) The average intensity of reaction zone at 5 minutes after dropping urine on the test strips. The fitting equation: average intensity = 152.3 − 2.286 × glucose concentration, with R^2 as 0.9973.

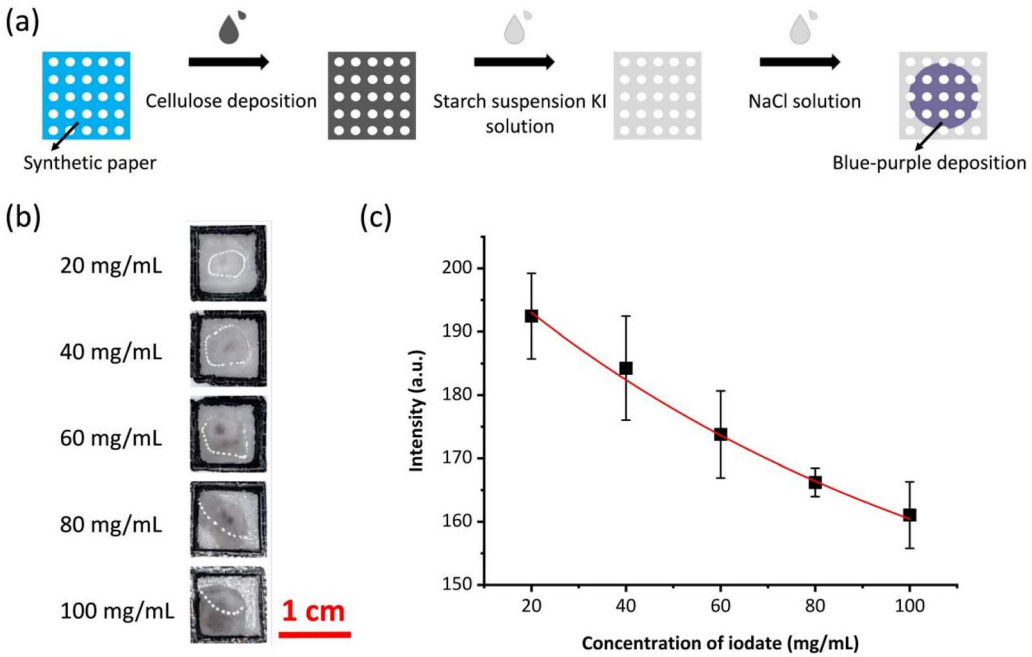

Fig. 6 Iodate detection in salt. (a) The experimental procedures of iodate detection in salt. (b) Images of test strips after testing salt solution with different iodate concentrations. (c) The average intensity of the blue-purple deposition when testing salt with different iodate concentrations. The fitting equation: average intensity = $73.65 \times \exp^{-\text{concentration of iodate}/104.2} + 132.3$, with R^2 as 0.9960.

and different concentrations of Tween 20. It can be seen that the flow rate is faster when the water just flows into the test strips, and gradually slows down as the distance increases, which aligns with that described by Washburn equation.[43] All fitting curves by Washburn equation of the distance–time plots show an excellent correlation with R^2 larger than 0.99.

Fig. 3(a) shows the physical view, schematic top view and side view of the water flow on the test strip. When the test strip is in contact with the green water solution, the water flows upward in the test strips by capillary action (see Fig. S4). In Fig. 3(b), it shows that water flows fastest on test strips by SP1, and the average flow rate is 0.0902 mm s^{-1}. With an average flow rate as 0.0769 mm s^{-1}, test strips by SP2 have the slowest flow rate among these three groups. The average flow rate is 0.0814 mm s^{-1} for the SP3 group. With the same length and width, test strip by SP1 has larger specific surface area than the

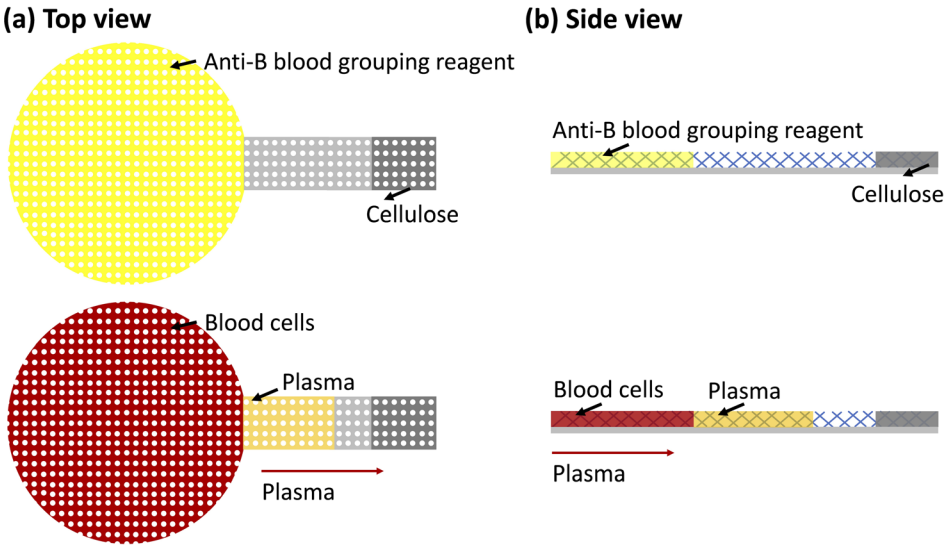

Fig. 7 Separation of plasma from whole blood on a test strip by the composite substrate. (a) Schematic top view of experimental procedures of plasma separation. The upper picture of (a) shows a test strip after coating agglutinating antibody on the sample area. The lower picture of (a) shows the plasma separation and collection at the end of plasma channel. (b) Schematic side view of experimental procedures of plasma separation. (c) Pictures of a test strip before and after adding whole blood samples.

other two, which will be more conducive for the immobilization of immuno reagents. Considering its high capillary flow rate and big specific surface area, we choose the composite substrate with SP1 to explore the influence of cellulose concentration and Tween 20 concentration in the following capillary flow experiments.

In Fig. 3(c), we find that water flows fastest on the test strips with highest cellulose concentration (100 mg mL^{-1}), and the average flow rate is 0.0902 mm s^{-1}. The average flow rate is 0.0492 mm s^{-1} for the test strips with 50 mg mL^{-1} cellulose solution. With an average flow rate as 0.0244 mm s^{-1}, the test strips with 25 mg mL^{-1} cellulose solution have the slowest flow rate among these three groups. This indicates that test strips patterned with higher concentration of cellulose will provide a faster capillary flow rate, which may be attributed to two reasons. On the one hand, a higher cellulose concentration increases the density of cellulose fibers within the porous structure of the OSTE synthetic paper, which in turn enhances the capillary forces that drive fluid movement. On the other hand, cellulose is inherently a hydrophilic material, and a higher concentration of cellulose may enhance the overall hydrophilicity of the substrate, thereby improving the liquid's ability to spread and penetrate within it.

As shown in Fig. 3(d), water flows fastest in the group with highest Tween 20 concentration (0.1%), and the average flow rate is 0.1514 mm s^{-1}. The average flow rate is 0.1013 mm s^{-1} for the group with 0.05% Tween 20. With an average flow rate as 0.0720 mm s^{-1}, the group with 0.02% Tween 20 provides the slowest flow rate among these three groups. This indicates that the greater the concentration of Tween 20, the faster the flow rate. As a hydrophilic surfactant, more Tween 20 (below the saturation concentration) will render the composite substrate more hydrophilic, thereby higher capillary flow rate.

Regarding the relatively low capillary flow rate ($\sim$0.1 mm s^{-1}) of the composite substrate, we recognize that the total flow time over a few centimeters may reach hundreds of seconds. However, this flow rate is comparable to that of many commercial slow-flow nitrocellulose membranes (*e.g.*, Millipore HF series), which are intentionally designed to enhance reaction sensitivity by prolonging analyte-reagent contact time. In addition, the flow rate can also be readily tuned by adjusting micropillar dimensions, cellulose concentration, or Tween 20 content to meet specific assay requirements. For evaporation-sensitive applications, a sealed cassette can be employed as in commercial LFT devices.

3.3 Spotting test on the composite substrate

Fig. 4 shows the results of spotting experiment. 0.25 μL, 0.35 μL and 0.50 μL water solutions with green color dye are dropped on various test strips, with different synthetic paper dimensions (SP1, SP2, and SP3), and different concentration of cellulose (25 mg mL^{-1}, 50 mg mL^{-1}, 100 mg mL^{-1}). In addition, the concentration of Tween 20 for the spotting experiments is 0.02%.

Fig. 4(a) shows the schematic diagram of the spotting test, and shows the diffusion of water on the test strip from the front and side. Fig. 4(b) shows pictures of the test strips after spotting test. We use a pipette to add a certain amount of water to the test strip, and the water diffuses and spreads on the test strip to form a spot. We observe the diffusion of water on different types of test strips and measure the area of spots.

In Fig. 4(c), we conduct the spotting tests on test strips with different concentrations of cellulose deposited (100 mg mL^{-1}, 50 mg mL^{-1} and 25 mg mL^{-1}). When 0.25 μL water is added on the test strips, the average areas are 0.1427 cm^2, 0.1618 cm^2, 0.1447 cm^2 for these test strips with cellulose concentration as 100 mg mL^{-1}, 50 mg mL^{-1} and 25 mg mL^{-1} respectively. When 0.35 μL water is added on the test strips, the average areas are 0.1684 cm^2, 0.2282 cm^2, 0.1766 cm^2 for these test strips with cellulose concentration as 100 mg mL^{-1}, 50 mg mL^{-1} and 25 mg μL^{-1} respectively. When 0.50 μL water is added on the test strips, the average areas are 0.2278 cm^2, 0.2862 cm^2, 0.2344 cm^2 for these test strips with cellulose concentration as 100 mg mL^{-1}, 50 mg mL^{-1} and 25 mg mL^{-1} respectively. The spot size increases with the volume of water. However, with the same volume, the spot size on the test strips with different concentrations of cellulose is quite different. The spot size on the test strips with 50 mg mL^{-1} cellulose is the largest. The spot size on the test strips with 100 mg mL^{-1} cellulose is slightly larger than that with 25 mg mL^{-1} cellulose.

As shown in Fig. 4(d), when 0.25 μL water is added on the test strips, the average areas are 0.1447 cm^2, 0.1126 cm^2, 0.1100 cm^2 for test strips by SP1, SP2, and SP3 respectively. When 0.35 μL water is added on the test strips, the average areas are 0.1766 cm^2, 0.1586 cm^2, 0.1802 cm^2 for test strips by SP1, SP2, and SP3 respectively. When 0.50 μL water is added on the test strips, the average areas are 0.2344 cm^2, 0.2435 cm^2, 0.2110 cm^2 for test strips by SP1, SP2, and SP3 respectively. The spot areas increase with the volume of water.

Considering the overall performance of microstructure, capillary flow rate, specific surface area and spotting area, we choose to use the composite substrate by SP1, 100 mg mL^{-1} cellulose, and 0.02% Tween 20 for the following applications including urine glucose detection, iodate detection of saline solutions, and plasma separation from whole blood. In addition, given the same area, the cost of this composite substrate is 8.3% lower than that of the commercial nitrocellulose membrane used in our lab (NC140C, Cobetter, Hangzhou, China).

3.4 Glucose detection in urine

After the test strip is prepared, the urine sample is added to one end of the non-reactive area of the test strip. Due to the action of capillary force, the urine would flow on the test strip and flow to the reaction area containing DAB and enzyme. When urine flows to the reaction area, after five minutes of reaction, the reaction area will produce a precipitation of stable dark brown. Fig. 5(a) and (b) show the experimental procedures of urine glucose detection. Fig. 5(c) shows the results of testing urine samples with different glucose concentrations (see Fig. S5(a)).

Fig. 5(d) shows the average intensity of blue channel of the reaction zone *versus* urine glucose concentration. Under the

catalysis of enzyme, glucose reacts with DAB reagent and generates brown precipitation.[44] Blue is the complementary color of brown. As the brown becomes darker, the intensity value of the blue channel decreases. The results show that the higher the concentration of glucose, the darker the color of the brown precipitation and the lower the intensity. The glucose detection concentration is clinically relevant and the linear fitting between intensity and glucose concentration has an excellent R^2 as 0.9973, making this test strip suitable for glucose detection at home or other POCT scenarios. Compared with methods using other substrates,[44,45] our approach exhibits a broader detection concentration range and better fitting performance. The substrate we employed demonstrates higher sensitivity in detecting urinary glucose while effectively reducing background noise interference.

It should be noted that this glucose detection system is an enzyme-based immunoassay, as it relies on specific immunoreagents—glucose oxidase (GOx) and horseradish peroxidase (HRP)—immobilized on the composite substrate to catalyze a chromogenic reaction with DAB. This demonstrates that the composite substrate is compatible with lateral flow immunoassay formats.

3.5 Iodate detection in salt

After preparing the iodate detection test strip, the salt solution containing iodate is added to the test strip. The solution diffuses on the test strip and reacts with the starch and KI on the test strip, which produces blue-purple precipitation. Fig. 6(a) shows the experimental procedures of iodate detection. Fig. 6(b) shows that different concentrations of iodate produce different blue-purple precipitation (see Fig. S5(b)). By detecting the gray intensity value of the blue-purple precipitation, we can build a relationship between gray intensity value with the iodate concentration. In Fig. 6(c), it can be seen that the average intensity steadily decreases when the concentration of iodate in NaCl solution increases. The reaction of starch with NaCl solution containing potassium iodate can produce blue-purple deposition,[46] which can be validated by the results that the higher the concentration of iodate, the smaller the intensity. The detection range is 20–100 mg mL^{-1} and the fitting between the iodate concentration and intensity is excellent with R^2 as 0.9960, which is promising for fast on-site detection of iodate in salt. We compared the performance of the method using this substrate with that of other substrates.[46,47] The concentration ranges for detection were similar, both spanning from 20 mg mL^{-1} to 100 mg mL^{-1}, and both exhibited good fitting results. Notably, for the colorimetric method, our grayscale values showed a broader range within the same detection range, indicating higher sensitivity to results at different concentrations.

3.6 Plasma separation from whole blood

In Fig. 7(a) and (b), it can be seen that the test strip can easily separate the plasma from whole blood. After the blood is added to the reaction area, it diffuses in the reaction area. Red blood cells in the sample area react with antibodies and agglutinate, and then stop flowing. Plasma flows through the narrow channel and reaches the collecting area. The result can be seen in Fig. 7(c). By implementing the same agglutination-based plasma separation strategy, plasma separation experiments are done on the commercial nitrocellulose membrane (NC140C, Cobetter) as a control experiment, which shows plasma separation with lower efficiency (see Fig. S6). In the future, we can enlarge the collecting area to increase the handling volume of whole blood and integrate immunoassays on the collecting area.

4 Conclusion

In this work, a LFT composite substrate is developed by patterning cellulose on OSTE synthetic paper. We perform capillary flow experiment and spotting test on this substrate to test its performance as LFT substrate. Moreover, in order to verify the potential of this composite substrate in the field of POCT, we successfully develop test strips based on this composite substrate to detect glucose concentration in urine, iodate concentration in food salt, and separate plasma from whole blood. The successful demonstration of an enzyme-based immunoassay for glucose detection indicates that this composite substrate holds strong potential for a wide range of lateral flow immunoassay applications, which is of particular significance to researchers and clinicians in point-of-care testing. Considering that the surface of OSTE has active chemical groups suitable for covalent bonding of antibodies, this composite substrate has great potential in LFT based on more complex immunoassays in the near future.

Author contributions

Qinghao He: investigation, data curation, methodology, writing. Jiahua Zhong: investigation, data curation, methodology, writing. Haonan Li: investigation, methodology. Xionghui Li: investigation, methodology. Yixi Shi: investigation, methodology. Muyang Zhang: investigation, methodology. Jie Zhou: investigation, methodology. Hao Chen: investigation, methodology. Xinyi Chen: investigation, methodology. Zhuoting Han: investigation, methodology, supervision. Lok Ting Chu: investigation, methodology, supervision. Huiru Zhang: investigation, methodology, supervision. Weijin Guo: conceptualization, investigation, methodology, writing, funding acquisition, supervision.

Conflicts of interest

There are no conflicts to declare.

Data availability

The data supporting this article have been included as part of the supplementary information (SI). Supplementary information: the fabrication of micropillar array, the cellulose dissolution experiments, the crack lengths of the composite substrate, pictures of test strips during experiments, images of urine

glucose and iodate detection experiments, and plasma separation on nitrocellulose membrane. See DOI: https://doi.org/10.1039/d6ra01317a.

Acknowledgements

This research was funded by National Natural Science Foundation of China (62404130, 62341403), Guangdong Basic and Applied Basic Research Foundation (2022A1515110855, 2026A1515011993), Department of Education of Guangdong Province (Scientific Research Project: 2022KQNCX019 and 2024KQNCX107), the Bureau of Education of Foshan City (Innovative Research Project: 2024SWYY03 and 2024SWYY04), National Excellent Engineer Innovation Research Institute for Advanced Manufacturing Industry in Guangdong Hong Kong Macao Greater Bay Area (Foshan) (Joint Training and Support Project: 2023FCXM016), Open Project funded by the MOE Key Laboratory of Tumor Molecular Biology, Jinan University, Guangzhou, China (2025 Open Project-202501), Guangdong Medical University (Start Funding: 4SG24241G), and Shantou University (STU Scientific Research Foundation for Talents: NTF20034).

References

1 M. Plebani, J. H. Nichols, P. B. Luppa, D. Greene, L. Sciacovelli, J. Shaw, A. I. Khan, P. Carraro, G. Freckmann, W. Dimech, *et al.*, *Clin. Chem. Lab. Med.*, 2025, **63**, 35–51.
2 J. H. Nichols, *EJIFCC*, 2021, **32**, 140.
3 C. M. Lilly, E. Ensom, S. Teebagy, D. DiMezza, D. Dunlap, N. Hafer, B. Buchholz and D. McManus, *Point Care*, 2020, **19**, 112–115.
4 H. R. Boehringer and B. J. O'Farrell, *Clin. Chem.*, 2022, **68**, 52–58.
5 J. Budd, B. S. Miller, N. E. Weckman, D. Cherkaoui, D. Huang, A. T. Decruz, N. Fongwen, G.-R. Han, M. Broto, C. S. Estcourt, *et al.*, *Nat. Rev. Bioeng.*, 2023, **1**, 13–31.
6 J. F. Bergua, L. Hu, C. Fuentes-Chust, R. Álvarez-Diduk, A. H. Hassan, C. Parolo and A. Merkoçi, *Lab Chip*, 2021, **21**, 2417–2426.
7 L. Willemsen, J. Wichers, M. Xu, R. Van Hoof, C. Van Dooremalen, A. Van Amerongen and J. Peters, *Biosensors*, 2022, **12**, 735.
8 W. Li, X. Yang, D. Wang, J. Xie, S. Wang and Z. Rong, *Talanta*, 2024, **277**, 126438.
9 E. Guler, T. Yilmaz Sengel, Z. P. Gumus, M. Arslan, H. Coskunol, S. Timur and Y. Yagci, *Anal. Chem.*, 2017, **89**, 9629–9632.
10 M. J. Raeisossadati, N. M. Danesh, F. Borna, M. Gholamzad, M. Ramezani, K. Abnous and S. M. Taghdisi, *Biosens. Bioelectron.*, 2016, **86**, 235–246.
11 S. G. Al-Shawi, E. K. Nasser, A. Kareem, M. Suliman, A. Shankar, S. Ray, P. Chaudhary, K. K. Sah, H. Abbasi and H. M. Hulail, *Microchem. J.*, 2025, 113978.
12 A. W. Martinez, S. T. Phillips, M. J. Butte and G. M. Whitesides, *Angew. Chem.*, 2007, **119**, 1340–1342.
13 Y. Zhang, A. K. Khan, D. See and J. Y. Ying, *ACS Appl. Mater. Interfaces*, 2023, **15**, 6561–6571.
14 A. K. Gashtroudkhani, M. D. Ghalehno, S. S. Abadi, M. Pouyani and A. Salimi, *Sci. Rep.*, 2025, **15**, 17470.
15 A. W. Martinez, S. T. Phillips, G. M. Whitesides and E. Carrilho, *Anal. Chem.*, 2010, **82**, 3–10.
16 A. Abbasi Moud, *Appl. Biosci.*, 2022, **1**, 1–37.
17 A. Manz, N. Graber and H. M. Widmer, *Sens. Actuators, B*, 1990, **1**, 244–248.
18 H. Lim, A. T. Jafry and J. Lee, *Molecules*, 2019, **24**, 2869.
19 S. Sachdeva, R. W. Davis and A. K. Saha, *Front. Bioeng. Biotechnol.*, 2021, **8**, 602659.
20 Y. Hou, C.-C. Lv, Y.-L. Guo, X.-H. Ma, W. Liu, Y. Jin, B.-X. Li, M. Yang and S.-Y. Yao, *J. Anal. Test.*, 2022, **6**, 247–273.
21 X. Jiang and Z. H. Fan, *Annu. Rev. Anal. Chem.*, 2016, **9**, 203–222.
22 K. Karimi, A. Fardoost, N. Mhatre, J. Rajan, D. Boisvert and M. Javanmard, *Micromachines*, 2024, **15**, 1274.
23 P. J. Lamas-Ardisana, P. Casuso, I. Fernandez-Gauna, G. Martínez-Paredes, E. Jubete, L. Añorga, G. Cabañero and H. J. Grande, *Electrochem. Commun.*, 2017, **75**, 25–28.
24 P. Lamas-Ardisana, G. Martínez-Paredes, L. Añorga and H. Grande, *Biosens. Bioelectron.*, 2018, **109**, 8–12.
25 J. Olkkonen, K. Lehtinen and T. Erho, *Anal. Chem.*, 2010, **82**, 10246–10250.
26 H. Shibata, Y. Hiruta and D. Citterio, *Analyst*, 2019, **144**, 1178–1186.
27 E. Carrilho, A. W. Martinez and G. M. Whitesides, *Anal. Chem.*, 2009, **81**, 7091–7095.
28 R. Ghosh, S. Gopalakrishnan, R. Savitha, T. Renganathan and S. Pushpavanam, *Sci. Rep.*, 2019, **9**, 7896.
29 G. Demirel and E. Babur, *Analyst*, 2014, **139**, 2326–2331.
30 T. Lam, J. P. Devadhasan, R. Howse and J. Kim, *Sci. Rep.*, 2017, **7**, 1188.
31 L. Cai, C. Xu, S. Lin, J. Luo, M. Wu and F. Yang, *Biomicrofluidics*, 2014, **8**, 5.
32 P. Ma, S. Wang, J. Wang, Y. Wang, Y. Dong, S. Li, H. Su, P. Chen, X. Feng, Y. Li, *et al.*, *Anal. Chem.*, 2022, **94**, 13332–13341.
33 C. Jönsson, M. Aronsson, G. Rundström, C. Pettersson, I. Mendel-Hartvig, J. Bakker, E. Martinsson, B. Liedberg, B. MacCraith, O. Öhman, *et al.*, *Lab Chip*, 2008, **8**, 1191–1197.
34 J. Melin, G. Rundström, C. Peterson, J. Bakker, B. D. MacCraith, M. Read, O. Öhman and C. Jönsson, *Anal. Biochem.*, 2011, **409**, 7–13.
35 G.-R. Han, H. J. Koo, H. Ki and M.-G. Kim, *ACS Appl. Mater. Interfaces*, 2020, **12**, 34564–34575.
36 Y. Liu, J. Li, Z. Xiao, T. Wu, C. Zhou and J. Zhou, *Small*, 2024, **20**, 2309956.
37 W. Xu, Z. Ren, L. Yang and Y. Cui, *Microchim. Acta*, 2025, **192**, 328.
38 J. Hansson, H. Yasuga, T. Haraldsson and W. Van der Wijngaart, *Lab Chip*, 2016, **16**, 298–304.
39 W. Guo, L. Vilaplana, J. Hansson, M.-P. Marco and W. van Der Wijngaart, *Biosens. Bioelectron.*, 2020, **163**, 112279.
40 W. Guo, J. Hansson and W. van der Wijngaart, *Anal. Chem.*, 2020, **92**, 6194–6199.

41 W. Guo, J. Hansson and W. van der Wijngaart, in *2021 IEEE 16th International Conference on Nano/Micro Engineered and Molecular Systems (NEMS)*, IEEE, 2021, pp. 1310–1313.
42 C. F. Carlborg, T. Haraldsson, K. Öberg, M. Malkoch and W. Van Der Wijngaart, *Lab Chip*, 2011, **11**, 3136–3147.
43 E. W. Washburn, *Phys. Rev.*, 1921, **17**, 273.
44 Z. Chen, H. Li, M. Zhang, X. Li, Y. Zhang, G. Zhu, Z. Feng, Z. Xiao, H. Zhang, X. Cui, *et al.*, *Microchem. J.*, 2024, **200**, 110423.
45 S. Kongkaew, S. Cotchim and W. Limbut, *Biosensors*, 2025, **15**, 688.
46 H. F. Galiga and F. B. Sevilla III, *Food Chem.*, 2023, **414**, 135741.
47 X. Li, X. Liang, H. Li, J. Song, K. Li, M. Zhang, H. Zhang, Z. Han, L. T. Chu and W. Guo, *Sens. Actuators Rep.*, 2025, 100323.